

## SWIFT AND FERMI OBSERVATIONS OF THE EARLY AFTERGLOW OF THE SHORT GAMMA-RAY BURST 090510

M. DE PASQUALE<sup>1\*</sup>, P. SCHADY<sup>1</sup>, N.P.M. KUIN<sup>1</sup>, M.J. PAGE<sup>1</sup>, P.A. CURRAN<sup>1</sup>, S. ZANE<sup>1</sup>, S.R. OATES<sup>1</sup>, S.T. HOLLAND<sup>2</sup>, A.A. BREEVELD<sup>1</sup>, E. A. HOVERSTEN<sup>3</sup>, G. CHINCARINI<sup>4,5</sup>, D. GRUPE<sup>3</sup>, *Fermi*/LAT AND *Fermi*/GBM COLLABORATIONS

<sup>1</sup>Mullard Space Science Laboratory, University College London, Holmbury St. Mary, Dorking, RH5 6NT, UK

<sup>2</sup>NASA/Goddard Space Flight Center, Greenbelt, MD 20771, USA

<sup>3</sup>Department of Astronomy & Astrophysics, Pennsylvania State University, 525 Davey Lab, University Park, PA 16802, USA

<sup>4</sup>Universita degli Studi di Milano Bicocca, Piazza della Scienza, 3, 20126 Milano, Italy

<sup>5</sup>Osservatorio Astronomico di Brera (INAF). Via E. Bianchi 46, 23807 Merate (LC), Italy

Draft version October 12, 2009

### ABSTRACT

We present the observations of GRB090510 performed by the *Fermi* Gamma-Ray Space Telescope and the *Swift* observatory. This is a bright, short burst that shows an extended emission detected in the GeV range. Furthermore, its optical emission initially rises, a feature so far observed only in long bursts, while the X-ray flux shows an initial shallow decrease, followed by a steeper decay. This exceptional behavior enables us to investigate the physical properties of the GRB outflow, poorly known in short bursts. We discuss internal shock and external shock models for the broadband energy emission of this object.

*Subject headings:* gamma rays: bursts

### 1. INTRODUCTION

With the availability of a relatively large sample of Gamma-Ray Bursts (GRBs), we came to recognize that they comprise of two large classes (Kouveliotou et al. 1993): the so-called short-hard GRBs (duration  $\lesssim 2$  s) and the long-soft ones ( $\gtrsim 2$  s). There is now increasing consensus that the observed dichotomy among long/short GRBs may indicate diverse initial physical conditions and progenitors. Long GRBs are associated with the demise of massive stars (Ferrero et al. 2006). Instead, short GRBs often occur in early-type galaxies (Zhang et al. 2009; Gehrels et al. 2009; Fong et al. 2009). This supports their interpretation in terms of compact object mergers.

Crucial information on GRBs is revealed by their afterglows, which can be monitored by *Swift* (Gehrels et al. 2004) in the optical and the X-ray range as soon as  $\sim 100$  s after the burst. In this paper, we present the study of the short GRB090510 with *Swift* and *Fermi* in a broad energy range, which extends from the optical up to a few GeV.

We report our observations and analysis in §2; in §3 we propose two different interpretations, in §4 we draw our conclusions. Hereafter, we use the conventions  $X = 10^n X_n$  for cgs units and  $F \propto t^{-\alpha} \nu^{-\beta}$ , where  $F$  is energy flux,  $t$  is the time from the trigger of *Swift* Burst Alert Telescope (BAT; Barthelmy et al. 2005a) and  $\nu$  the frequency. Errors are reported at  $1\sigma$ , unless otherwise specified. We assume a cosmology in which  $H_0 = 71$  km s<sup>-1</sup> Mpc<sup>-1</sup>,  $\Omega_m = 0.27$ ,  $\Omega_\lambda = 0.73$ . All the fluxes, times and frequencies are measured in the observer's frame.

### 2. OBSERVATIONS AND DATA ANALYSIS.

#### 2.1. BAT data

At 00:23:00 UT, May 10th, 2009, BAT, which operates in the 15-350 keV range, triggered on GRB090510 (Hoversten et al. 2009). *Swift* slewed immediately to the burst. The duration was  $T_{90} = 0.30 \pm 0.07$  s. Detailed analysis of the BAT data is shown in Ukwatta et al. (2009).

#### 2.2. XRT data

The *Swift* X-ray Telescope (XRT; 0.3-10 keV; Burrows et al. 2005) began to observe the X-ray afterglow of GRB090510 at T+98 s. The lightcurve (Fig. 1) shows an initial slow flux decline. Observations were interrupted when the source entered the Earth constraint at T+1.9 ks. When they resumed, at T+5.1 ks, the flux was much lower. A broken powerlaw fit of the lightcurve gives as best fit parameters an early decay slope  $\alpha_{X,1} = 0.74 \pm 0.03$ , break time  $t_X = 1.43^{+0.09}_{-0.15}$  ks, late decay slope  $\alpha_{X,2} = 2.18 \pm 0.10$ ;  $\chi^2 = 112$  with 77 degrees of freedom (d.o.f.), which is still marginally acceptable (chance probability  $P = 0.0054$ ).

#### 2.3. UVOT and other optical data

The *Swift* Ultra Violet and Optical Telescope (UVOT; 160-800 nm; Roming et al. 2005; Poole et al. 2008) began settled exposures at T+97 s. The lightcurve of the optical afterglow, produced by renormalizing all individual filters to white, as described in Oates et al. (2009), is shown in Fig. 1. The optical emission rises until  $\sim 1.6$  ks, then decays. The optical lightcurve is well fitted ( $\chi^2 = 23.9$  with 19 d.o.f.) by a broken powerlaw (Beuermann et al. 1999) with a smooth break. The best fit parameters are:  $\alpha_{Opt,1} = -0.50^{+0.11}_{-0.13}$ ;  $t_{peak} = 1.58^{+0.46}_{-0.37}$  ks;  $\alpha_{Opt,2} = 1.13^{+0.11}_{-0.10}$ . Adding a constant does not improve the fit significantly, suggesting a small host galaxy contribution. Very Large Telescope observations (Rau et al. 2009) provide a spectroscopic redshift of

\*Corresponding authors: M. De Pasquale: mdp@mssl.ucl.ac.uk; M. J. Page: mjp@mssl.ucl.ac.uk; K. Toma: toma@astro.psu.edu; V. Pelassa: Veronique.Pelassa@lpta.in2p3.fr.

$z = 0.903$ . Using this redshift and the *Fermi* spectral parameters, the isotropic equivalent energy of GRB090510 is  $E_{iso} = 1.08 \times 10^{53}$  ergs in the 10 keV - 30 GeV rest frame (Abdo et al. 2009).

#### 2.4. *Fermi* data

GRB090510 triggered both instruments on-board the *Fermi* observatory (Guiriec et al. 2009; Ohno, & Pelassa 2009). The Gamma-ray Burst Monitor (GBM; 8 keV - 40 MeV) observed the burst during the prompt emission phase, and after an autonomous re-pointing, the Large Area Telescope (LAT; 20 MeV - more than 300 GeV) began observations and detected a long-lasting (up to 200s) high-energy (up to 4 GeV) emission. The analysis and interpretation of the prompt emission is presented in Abdo et al. (2009). Follow up observations lasted until 1500 s when the source was occulted by the Earth, and resumed  $\sim 3.5$  ks later. The observation epochs are defined in Table 1. A time-resolved spectral analysis using diffuse events (Atwood et al. 2009) was performed (Table 1). The spectrum shows no significant evolution, and it is well-fitted by a powerlaw with energy index  $\beta_\gamma = 1.1 \pm 0.1$ . The lightcurve shows no significant feature and is best fitted by a powerlaw. The onset of the GBM emission (T+0.013 s) is a sensible reference for this temporal fit and yields a decay index  $\alpha_\gamma = 1.38 \pm 0.07$  ( $\chi^2/\text{dof} = 9.4/7$ ) (Fig. 1). For the binned spectral analysis described in §3.2, transient events from an energy-dependent region of interest were used, and front and back events were treated separately (Atwood et al. 2009).

### 3. DISCUSSION

GRB090510 was a short burst with a relatively bright afterglow, and  $E_{iso}$  is among the highest for this class (Graham et al. 2009). The early rise of the optical flux is so far unique in short GRBs. More importantly, GRB090510 shows high energy emission up to the GeV range, until T+200 s.

Energetic short GRBs with optical transients, such as GRB050724 (Barthelmy et al. 2005b), typically have extended emission (EE) detected by BAT and XRT, following the hard emission spike (Troja et al. 2008). If GRB090510 had occurred at  $z = 0.26$ , as GRB050724, it would have produced a flux in the BAT range of a few  $10^{-9}$  ergs  $\text{cm}^{-2}$   $\text{s}^{-1}$  until  $\sim 100$  s, and we would have classified it as an EE-GRB.

The nature of this high energy emission is nevertheless not easy to understand. EE often fades slowly for a few hundreds of seconds, then vanishes with a slope which can be as fast as  $\alpha \sim 7$ ; after this sudden drop a late afterglow with a typical decay slope  $\alpha \sim 1.4$  is sometimes observed (e.g. GRB050724; GRB080123, Mangano et al., 2008). The fast decay and the extrapolation of the late afterglow back to early epochs suggest that EE is not the onset of the late afterglow (Nakar 2007). Furthermore, in a few cases where the EE is bright enough to be studied in detail (Norris & Bonnell 2006), it is found to have variations too rapid to be explained with external shock models (Mészáros & Rees 1993). EE might instead indicate a declining activity of the GRB central engine (Rosswog 2007; Metzger et al., 2008; Perna et al. 2006; Goad et al. 2007); once this activity ends, then falls abruptly, and the forward shock (FS) emission prevails.

In other cases, however, the flux decay from the beginning of *Swift* observations seems due to the usual FS mechanism, such as in GRB051221 (Burrows et al. 2006) and GRB 061201 (Stratta et al. 2007).

We propose and discuss separately 2 scenarios to explain the emission after the initial spike: in the first one, the emission is due to both external FS and internal shock, (IS, Rees & Mészáros 1994) while in the second the emission is due to FS alone.

#### 3.1. *X-ray internal shock, optical external shock*

In the first scenario we assume that the initial X-ray (until the break at  $\sim 1.4$  ks) and  $\gamma$ -ray flux are IS emission, while the FS is responsible for the optical lightcurve and the late X-ray flux. In particular, the optical rise may be due to the onset of FS emission, detected  $10^2 - 10^3$  s after the trigger in long GRBs (Oates et al. 2009). This model can explain the different behavior of the early X-ray/LAT and optical lightcurves.

We constrain some physical properties of the FS blastwave. The initial Lorentz factor of the ejecta is  $\Gamma_0 = 1.4 \times 10^2 E_{53}^{1/8} n^{-1/8} t_{peak,3}^{-3/8}$  (Sari 1997), where  $E$  is the isotropic kinetic energy,  $n$  the environment density in  $\text{cm}^{-3}$ , and  $t_{peak}$  is the peak time. The maximum FS flux is at the synchrotron characteristic frequency  $\nu_m$ , and it is  $F_{\nu_m} = 1.3 \times 10^4 E_{53} \epsilon_{B,-2}^{1/2} n^{1/2} \mu\text{Jy}$  (Granot & Sari 2002), where  $\epsilon_B$  is the fraction of internal energy in the magnetic field.

These parameter values must be consistent with  $\Gamma_0 \gtrsim 1000$  (Abdo et al. 2009) and with the UVOT data, which give a  $3\sigma$  lower limit on  $t_{peak} > 730$  s and a peak flux  $F \simeq 100 \mu\text{Jy}$ . The first constraint can be written  $E_{53} n^{-1} > 2.6 \times 10^6$ . If  $\nu_m$  is just below the optical band, the constraint on the flux becomes  $E_{53} \epsilon_{B,-2}^{1/2} n^{1/2} \simeq 7.7 \times 10^{-3}$ . Assuming  $\epsilon_{B,-2} \simeq 1$ , the model is consistent with observations for  $E_{53} \gtrsim 5.4$ , while  $n \simeq 5.9 \times 10^{-5} E_{53}^{-2}$ .

The XRT and LAT fluxes can be explained by IS synchrotron emission with  $\nu_c < \nu_{Opt} < \nu_{sa} < \nu_X < \nu_m$ , where  $\nu_c$  is the synchrotron cooling frequency and  $\nu_{sa}$  is the synchrotron self-absorption frequency (Guetta & Granot 2003). The synchrotron luminosity, estimated from the 100s spectral energy distribution (SED, Fig. 2), is  $L \simeq 10^{50}$  erg  $\text{s}^{-1}$ . We find that for this value of  $L$  and for  $p = 2.4$ ,  $\epsilon_{e,-1} = 5.5$ ,  $\epsilon_{B,-2} = 33$ ,  $\Gamma = 410$ ,  $t_v = 3 \times 10^{-5}$  s, where  $p$ ,  $\epsilon_e$ ,  $\Gamma$  and  $t_v$  are the index of the powerlaw electron energy distribution, the fraction of energy given to electrons, the bulk Lorentz factor and the variability timescale respectively, we have  $\nu_m \simeq 210$  keV,  $F(1.7 \text{ keV}) \simeq 75 \mu\text{Jy}$ , which is within a factor  $\sim 3$  from the observations, and  $F(100 \text{ MeV}) \simeq 4.2 \times 10^{-3} \mu\text{Jy}$ , which is consistent within  $2\sigma$  of the data. The cut-off energy for pair production is  $h\nu_{\gamma\gamma} \simeq 1.6$  GeV, thus allowing the late emission of  $\sim 1$  GeV photons. IS does not produce detectable emission in the optical, since this is below  $\nu_{sa} \simeq 0.32$  keV.

Compared with the scenario presented in §3.2, this model has the advantage of not requiring extreme values of  $\Gamma_0$  to explain an early (few seconds) FS emission onset in a low density environment expected for a short burst. However, it needs some fine tuning of parameters. The optical rise slope  $\alpha_{Opt,1} = -0.5$  is shallower than that expected at the FS onset ( $\alpha = -2$ ), although

similar slow rises have been observed (Oates et al. 2009). It is possible that the onset of our observations caught the end of this steep rise phase, when the afterglow was turning over to a decay. Another possible problem is that the required density appears very low. We note that the observed slope would be expected if  $\nu_m$  were crossing the optical band and, in general, broad FS onset rises are also expected for outflows observed off-axis (Panaitescu & Verstrand 2008). However, a bright and hard event such as GRB090510 is difficult to reconcile with the latter scenario, which predicts soft and dim prompt emission (Yamazaki et al. 2002).

### 3.2. Optical, X-ray and GeV emission from external shock.

A second possibility is that the afterglow of GRB090510, including the emission detected by LAT, is entirely produced by the FS propagating in a constant density medium (Sari et al. 1998). According to the model, the broad afterglow spectrum<sup>1</sup> consists of three segments: a low-energy tail, of spectral slope  $\beta_1 = -1/3$ ; another segment, for  $\nu_m < \nu < \nu_c$ , where  $\beta_2 = (p-1)/2$ ; blueward of  $\nu_c$ , the third segment has  $\beta_3 = p/2$ . For comparison with this spectral template, we built up 5 SEDs, at 100 s, 150 s, 1 ks, 7 ks, and 12 ks (Fig. 3), all including UVOT and XRT data, and LAT data were also included in the first SED. LAT data were accumulated between 10 s and 200 s (i.e. well after the end of the prompt emission seen in the GBM), and renormalized to 100 s using the decay index of  $\alpha_\gamma = 1.38$ . We fitted the SEDs simultaneously with a double broken powerlaw model, forcing  $\beta_1 = -1/3$  and  $\beta_3 = \beta_2 + 1/2$ . We allowed the breaks to vary and Galactic and host extinction were accounted for. The result is acceptable ( $\chi^2/\text{d.o.f.} = 110.3/83$ ) and is shown in Fig. 3 and Table 2. The FS alone could successfully describe the spectrum over 9 decades of frequency. A break between X-ray and  $\gamma$ -ray ranges is fitted, at  $E_2^b \simeq 300$  MeV, but not constrained. It is studied more precisely by fitting the 100 s SED alone, freezing  $N_H$  and  $E(B-V)$  at the 5 SEDs fit results and leaving  $\beta_2$  and  $\beta_3$  free to vary (see Table 2). This fit fulfills the relation  $\beta_3 = \beta_2 + 1/2$  (at  $1.3\sigma$ ) and a significant break is found ( $3.6\sigma$ ), although it yields a slightly harder  $\beta_2$  ( $1.8\sigma$ ) than the 5 SED fit shown in Fig. 3. The LAT emission shows no spectral evolution, even at early times. Therefore, to better characterize the high-energy spectrum, the SED at 100 s was rebuilt including LAT data between 0.38 s and 200 s (see Table 2 and Fig. 2). A significant break ( $> 4.5\sigma$  including systematics) between 10 and 133 MeV was found. However, including this selection of LAT data in the 5 SED fit yields a worse fit ( $\chi^2/\text{dof} = 125.3/83$ ) than that shown in Fig. 3.

In this FS interpretation, the initial increase of the optical emission is due to  $\nu_m$  approaching the optical band. The X-ray is already decaying because it lies above  $\nu_m$ . In order to verify whether the required physical parameters are plausible, we impose the following constraints: i)  $F(1 \text{ ks}) \simeq 2.2 \mu\text{Jy}$  at  $10^{18}$  Hz and ii)  $\nu_m(1 \text{ ks}) \simeq 10^{16}$  Hz. Adopting the expressions for  $F_{\nu_m}$ ,  $\nu_m$ , and  $\nu_c$  from Granot & Sari (2002), the constraints above lead to

the following equations:  $\epsilon_{B,-2} \simeq 14 E_{53}^{-1/2} \epsilon_{e,-1}^{-4} \xi_p^{-4} \nu_{os}^2$ ,  $n \simeq 1.5 \times 10^{-6} (1330)^{p-2.5} E_{53}^{-1} \epsilon_{e,-1}^4 \xi_p^4 \nu_{os}^{-p-1}$ , where  $\xi_p = 3(p-2)/(p-1)$  and  $\nu_{os} = \nu_m(1 \text{ ks})/10^{16}$  Hz. We verified that the synchrotron self-Compton cooling is not significant for  $t \leq 1.5$  ks and  $\nu_c(1.5 \text{ ks}) > 10^{18}$  Hz for a reasonable range of parameters (Nakar et al. 2009). A very low, but not implausible, density is suggested.

The flux at 100MeV is

$$F_{\nu > \nu_c} \simeq 2.4 \times 10^{-3} (2.2 \times 10^{-3})^{(p-2.5)} E_{53} \epsilon_{e,-1} (t/100\text{s})^{(2-3p)/4} (h\nu/100\text{MeV})^{-p/2} \xi_p \nu_{os}^{(p-2)/2} \mu\text{Jy} \quad (1)$$

This is consistent with the LAT data at 100s, provided  $E_{53} \epsilon_{e,-1} \simeq 5$ ,  $p \approx 2.5$ ,  $\xi_p \approx 1$ , and  $\nu_{os} \approx 1$ . For these parameters,  $\nu_c \ll 4\text{GeV}$  at  $t \gtrsim 1$  s, so that the flux in the LAT energy range is approximated to be  $F \propto t^{(2-3p)/4} \sim t^{-1.4}$  at  $t \gtrsim 1$  s, consistent with the LAT light curve. We note that  $\Gamma_0 > 5800 E_{53}^{1/8} n^{-1/8}$  is required for the FS onset time to be  $\lesssim 1$  s.

In summary, the spectral properties of GRB 090510 could be explained by a simple FS model. We note, though, that this simple model is hard to reconcile with some of the observed temporal properties. Firstly, it predicts an X-ray decay index before the break of  $\alpha = 3\beta_2/2 = 1.16 \pm 0.06$ , clearly inconsistent with the observed  $\alpha_{X,1} = 0.74 \pm 0.03$ . Secondly, if the X-ray break at  $t = 1.4$  ks is attributed to a jet break (Sari et al. 1999) and, after this time, optical and X-ray lie on the same spectral segment, then the asymptotic optical decay index should be the same as  $\alpha_{X,2} = 2.18 \pm 0.10$ . However, a fit of the whole lightcurve with a smooth broken power-law (§2.3), adding a constant (as a host galaxy contribution), gives an asymptotic decay slope  $\alpha_{Opt,2} = 1.13_{-0.09}^{+0.17}$ , incompatible with the X-ray decay. Finally, although the error bars are quite large, we notice that, taken at face value, the slope of the UVOT spectrum in the 1 ks SED is negative (Fig. 3), suggesting that  $\nu_m$  may be already below the optical at that epoch.

The above mentioned flaws imply that the simple FS model is not viable to explain the properties of GRB090510. However, this model relies on highly idealized assumptions, and it is known that several GRB afterglows do not strictly follow its simple predictions. Plausible effects that may affect the predictions and ease the comparison with GBR090510 are:

- a phase of energy injection (Sari & Mészáros 2000), or an evolution of the microphysical parameters of the blast wave (Panaitescu et al. 2006); both may cause an early shallow decay of the X-ray flux;
- the transit of  $\nu_m$  slightly after the jet break, which could explain a shallow late optical decay.

With the present data, we are unable to distinguish between energy injection and microphysical parameter evolution. As for the X-ray decay post jet break, hydrodynamical simulations show that initially the jet decay slope can reach  $\alpha \simeq 3$  (Granot 2007). Both the processes of energy injection and parameter evolution are capable of keeping the decay shallower, so that a late X-ray decay slope of  $\alpha_{X,2} = 2.18 \pm 0.10$  could be achieved. Therefore, with some extensions, the FS model could arrange the temporal properties, although some fine tunings would be needed.

<sup>1</sup> The self-absorption frequency is not relevant in this study.

## 4. CONCLUSIONS

We have reported the *Swift* and *Fermi* observations of the short GRB090510, an event endowed with bright prompt and afterglow emission, and detected in the GeV range up to 200 s after the trigger. The initial X-ray emission shows a slow decay up to  $\simeq 1.4$  ks, after which it quickly drops. The optical flux peaks at  $\simeq 1.6$  ks. We have explored two scenarios to explain the observed behaviors.

In the first scenario, the early flux detected by XRT and LAT is due to IS, while the optical rise is the onset of FS emission or the transit of  $\nu_m$ . This interpretation does not require extremely high values of Lorentz factor, should the density of the environment be very low. We also find that reasonable values for the physical parameters can lead to the observed properties, which might favour the model, although some fine tuning is necessary. The second scenario assumes that the FS produces the full spectrum of the emission, observed from the optical to the GeV band. The  $\gamma$ -ray, X-ray and optical spectrum can be reproduced by the template FS spectral model and the required physical parameters are plausible. Although the simple FS model fails to reproduce

the observed temporal behavior, extensions of this model could accommodate the temporal mismatch. In order to identify the origin of the GeV component of GRBs like 090510, more case studies will be necessary. Fortunately, we have very promising prospects for other simultaneous *Fermi* and *Swift* observations of short GRBs, which will provide us with more measurements to shed light on the properties of this class of events.

The *Fermi* LAT Collaboration acknowledges support from a number of agencies and institutes for both development and the operation of the LAT as well as scientific data analysis. These include NASA and DOE in the United States, CEA/Irfu and IN2P3/CNRS in France, ASI and INFN in Italy, MEXT, KEK, and JAXA in Japan, and the K. A. Wallenberg Foundation, the Swedish Research Council and the National Space Board in Sweden. Additional support from INAF in Italy and CNES in France for science analysis during the operations phase is also gratefully acknowledged. SZ acknowledges STFC support. This work used data supplied by the UK Swift SDC at the University of Leicester.

## REFERENCES

- Abdo A.A., et al. 2009, in preparation  
 Atwood, W., Abdo, A. A., Ackermann, M., et al. 2009 ApJ, 697, 1071  
 Barthelmy, S.D., Barbier, L.M., Cummings, J.R., et al. 2005, SSRv, 120, 143  
 Barthelmy, S.D., Chincarini, G., Burrows, D.N., et al. 2005, Nature, 438, 944  
 Beuermann, K., Hessmann, F.V., Reinsch K. et al. 1999, A&A, 352, 26  
 Burrows, D.N., Hill, J.E., Nousek, J.A., et al. 2005, SSRv, 120, 165  
 Burrows, D.N., Grupe, D., Capalbi, M., et al. 2006, ApJ, 653, 468  
 Evans, P.A., Beardmore, A.P., Page, K.L. et al. 2007, A&A 469, 379-385  
 Evans P.A., Beardmore, A.P., Page K.L., et al. 2009, MNRAS submitted, arXiv:08123662  
 Ferrero P., Kann, D.A., Zeh, A., et al. 2006, A&A 457, 857  
 Fong, W., Berger, E., & Fox, D. B. 2009, ApJ, submitted, arXiv:0909.1804  
 Gehrels, N., Chincarini, G., Giommi P., et al. 2004, ApJ, 611, 1055  
 Gehrels, N., Ramirez-Ruiz, E., & Fox, D. S. 2009, ARAA, 47, 567  
 Graham, J. F., Fruchter, A. S., Levan, A. J., et al. 2009, ApJ, 698, 1620  
 Goad, M.R., Page K.L., Godet, O., et al 2007, A&A, 468, 103  
 Granot J. 2007, RMAC, 27, 140  
 Granot, J., & Sari, R. 2002, ApJ, 568, 820  
 Guetta, D., & Granot, J. 2003, ApJ, 585, 885  
 Guiriec, S., Connaughton, V. & Briggs M. 2009, GCN 9336  
 Hoversten, E.A., Krimm, H.A., Grupe, D. et al. 2009, GCN 9331  
 Kouveliotou, C., Meegan, C.A., Fishman, G.J. et al. 1993, ApJ, 413, 101  
 Mangano V., Sbarufatti, B., Ukwatta, T.N., et al. 2008, GCN 7208  
 Mészáros P & Rees M. 1993, ApJ405, 278  
 Metzger, B.D., Quataert, E. Thompson, T. A. 2008, MNRAS, 385, 1455  
 Nakar E. 2007, PhR, 442, 166  
 Nakar E., Ando, S., Sari, R. 2009, arXiv:0903.2557  
 Norris, J.P., & Bonnel, J.T. 2006, ApJ, 643, 266  
 Oates, S.R., Page, M. J., Schady, P. et al. 2009 MNRAS395, 490  
 Ohno, M. & Pelassa, V. 2009, GCN 9334  
 Panaitescu A., Mészáros, P., Burrows, D., et al. 2006, MNRAS, 369, 2059  
 Panaitescu A. & Vestrand T. 2008, MNRAS, 387, 479.  
 Perna, R. Armitage, P. J., Zhang, B. 2006, ApJ, 636, 29  
 Poole, T.S., Breeveld, A.A., Page, M.J., et al. 2008, MNRAS, 383, 627  
 Rau A., McBreen S., Kruehler T. et al. 2009, GCN 9353  
 Rees, M. J. & Meszaros, P. 1994, ApJ, 430, 93  
 Roming, P.W.A., Kennedy, T.E., Mason, K.O., et al. 2005, SSRv, 120, 95  
 Rosswog, S. 2007, RMxAC, 27, 57R  
 Sari, R. 1997, ApJ, 489, 37  
 Sari, R., & Mészáros P. 2000, ApJ, 535, 33  
 Sari, R., Piran, T., & Narayan R. 1998, ApJ, 497, 17  
 Sari, R., Piran., T., and Heger, J. 1999, ApJ, 519, 17  
 Stratta, G., D'Avanzo, P., Piranomonte, S. et al. 2007, A&A, 474, 827  
 Troja, E., King, A.R., O'Brien, P.T. et al. 2008, MNRAS, 385, 10.  
 Ukwatta., T.N., Barthelmy, S.D., Baumgartner W.H. et al. 2009, GCN 9337  
 Yamazaki, R., Ioka, K., & Nakamura, T. 2002, ApJ, 571, 31  
 Zhang, B., Zhang, B.-B., Virgili, F. J. et al. 2009, ApJ in press, arXiv:0902.2419.

Time bins (s)	Test Statistic	Energy index	Photon flux above 100 MeV ( $ph.cm^{-2}.s^{-1}$ )
1: 0.38 – 0.48	208.2	$0.85_{-0.26}^{+0.30}$	$2.49_{-0.84}^{+1.13} 10^{-2}$
2: 0.48 – 0.92	541.8	$1.20_{-0.20}^{+0.22}$	$1.89_{-0.39}^{+0.46} 10^{-2}$
3: 0.92 – 1.5	192.1	$0.93_{-0.26}^{+0.30}$	$5.7_{-1.8}^{+2.4} 10^{-3}$
4: 1.5 – 2.5	301.7	$1.41_{-0.28}^{+0.31}$	$6.4_{-1.6}^{+2.0} 10^{-3}$
5: 2.5 – 5.5	163.	$0.76_{-0.22}^{+0.26}$	$8.4_{-2.7}^{+3.6} 10^{-4}$
6: 5.5 – 11.5	58.	$0.86_{-0.35}^{+0.44}$	$2.0_{-0.9}^{+1.4} 10^{-4}$
7: 11.5 – 37.	71.	$2.27_{-0.59}^{+0.70}$	$1.67_{-0.82}^{+0.99} 10^{-4}$
8: 37. – 69.5	59.9	$0.85_{-0.32}^{+0.39}$	$4.4_{-1.8}^{+2.6} 10^{-5}$
9: 69.5 – 200.	43.	$1.74_{-0.71}^{+0.58}$	$1.6_{-0.7}^{+1.0} 10^{-5}$
10: 200. – 400.	$\sim 0.$	1.1 / 0.5 / 2.5	$< 4.7 / 3.2 / 7.9 10^{-6}$
11: 400. – 800.	$\sim 0.$	1.1 / 0.5 / 2.5	$< 2.3 / 1.6 / 3.9 10^{-6}$
12: 800. – 1500.	$\sim 0.$	1.1 / 0.5 / 2.5	$< 2.1 / 1.2 / 3.8 10^{-6}$
13: 4200. – 7200.	$\sim 0.$	1.1 / 0.5 / 2.5	$< 0.48 / 0.3 / 1.0 10^{-6}$
14: 10150. – 13000.	$\sim 0.$	1.1 / 0.5 / 2.5	$< 0.47 / 0.3 / 0.9 10^{-6}$
15: 15800. – 18500.	$\sim 0.$	1.1 / 0.5 / 2.5	$< 0.52 / 0.3 / 1.0 10^{-6}$

TABLE 1

LAT TIME-RESOLVED SPECTROSCOPY. THE SOURCE TEST STATISTIC WAS DEFINED AS TWICE THE DIFFERENCE OF THE UNBINNED LOG-LIKELIHOOD BETWEEN THE NULL HYPOTHESIS (BACKGROUND ONLY) AND THE ALTERNATIVE HYPOTHESIS (PRESENCE OF A SOURCE). BOTTOM TABLE SHOWS 95% CONFIDENCE LEVEL UPPER LIMITS ON FLUX FOR DIFFERENT ENERGY INDECES.

SED LAT dataset (s)	5 SED 10. – 200.	100 s 10. – 200.	100 s 0.38 – 200.
$N_H$ ( $\times 10^{21} \text{ cm}^2$ )	$1.52_{-0.30}^{+0.33}$	1.52 (fixed)	1.52 (fixed)
$E(B - V)$ (mag)	$0.000_{-0.000}^{+0.005}$	0. (fixed)	0. (fixed)
$E_1^b$ (keV)	$\left\{ \begin{array}{l} 0.43_{-0.07}^{+0.10} \text{ (100 s)} \\ 0.17_{-0.02}^{+0.03} \text{ (150 s)} \\ 0.037_{-0.007}^{+0.005} \text{ (1000 s)} \\ < 0.001 \text{ (7000 s)} \\ < 0.01 \text{ (12000 s)} \end{array} \right.$	$0.31_{-0.06}^{+0.05}$	$0.31_{-0.05}^{+0.06}$
$\beta_2$	$0.77 \pm 0.04$	$0.61_{-0.10}^{+0.06}$	$0.62_{-0.06}^{+0.08}$
$E_2^b$ (MeV)	$\simeq 300$ (100 s)	[20 – 135]	[10 – 133]
$\beta_3$	$\beta_2 + 1/2$	$1.44_{-0.22}^{+0.26}$	$1.14_{-0.09}^{+0.10}$

TABLE 2

BEST FIT PARAMETERS OBTAINED BY FITTING THE 5 SEDS SIMULTANEOUSLY OR THE SED AT 100 S ONLY WITH A DOUBLE BROKEN POWERLAW MODEL (SEE TEXT).  $N_H$  AND  $E(B - V)$  ARE HOST ABSORPTION AND EXTINCTION RESPECTIVELY;  $E_1^b$  AND  $E_2^b$  ARE THE TWO BREAK ENERGIES CALCULATED AT THE EPOCH IN PARENTHESIS.

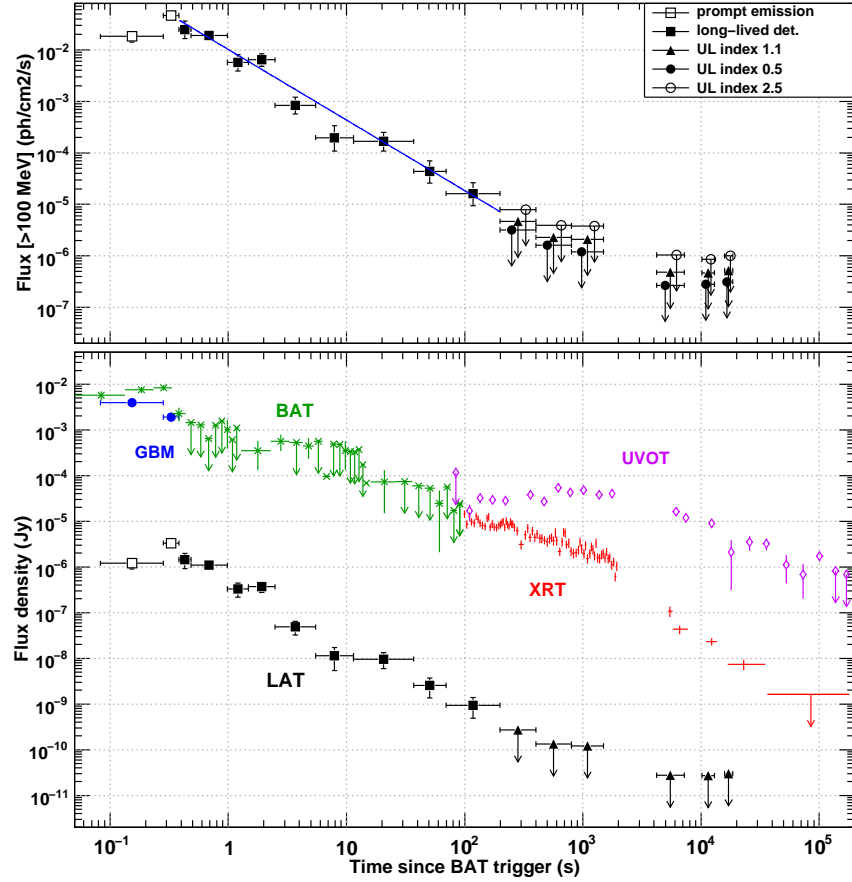


FIG. 1.— **Top:** LAT flux above 100 MeV and best fit to the flux decay (line). **Bottom:** energy flux densities averaged in the observed energy bands: BAT (15 keV – 350 keV, stars); XRT (0.2 keV – 10 keV, crosses); UVOT renormalised to white (diamonds); LAT (100 MeV – 4 GeV, filled squares); the average spectral index was used to convert from photon to energy flux) with upper limits for  $\beta = 1.1$  (triangles). The prompt emission is shown for comparison: GBM (8 keV – 1 MeV, circles), LAT (100 MeV – 4 GeV, empty squares). XRT lightcurve is obtained as in Evans et al. (2007, 2009). All data are shown with 68% error bars or 95% confidence level upper limits.

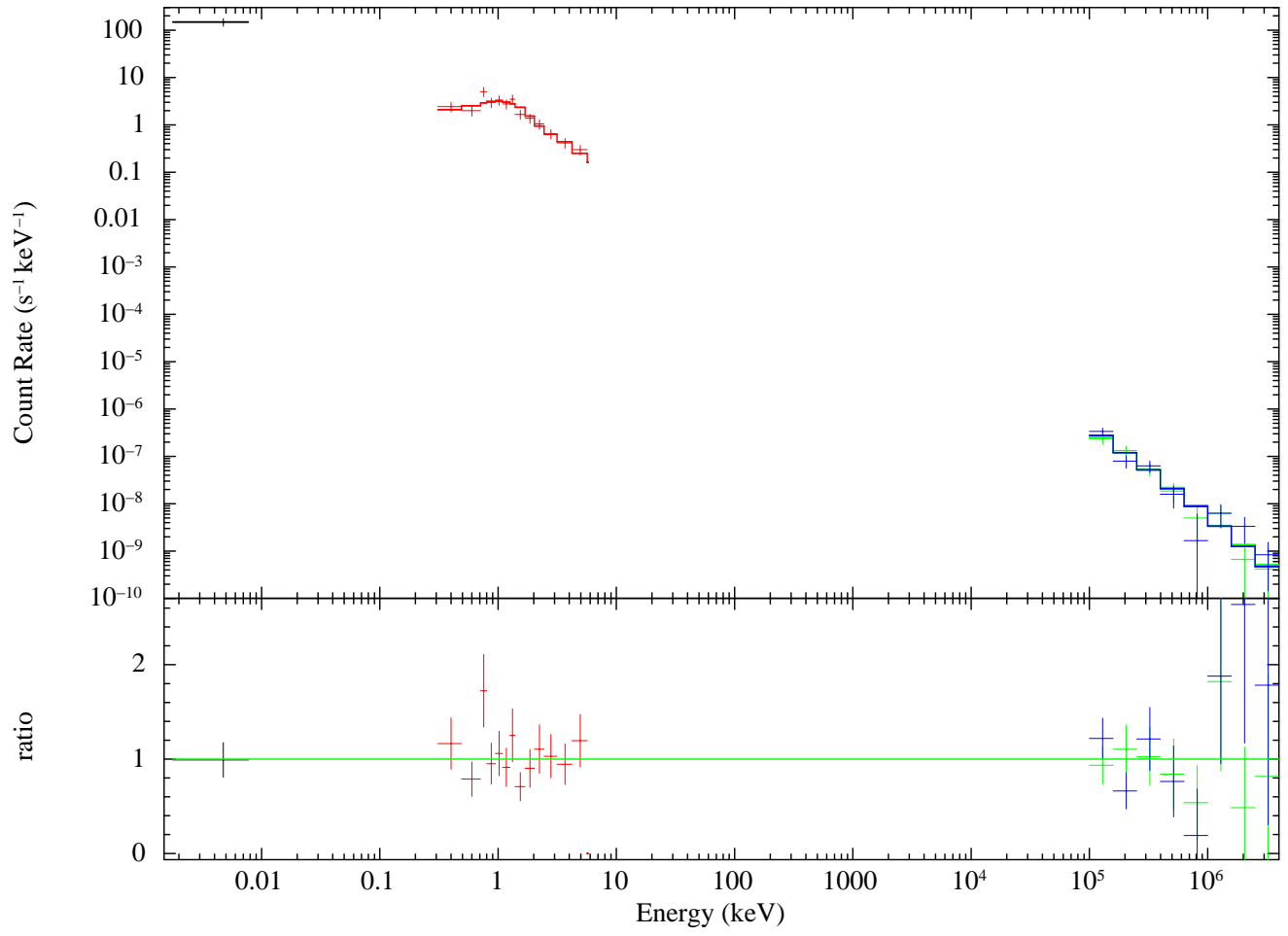


FIG. 2.— UVOT-XRT-LAT count spectrum, with best fit and residuals shown (see text)

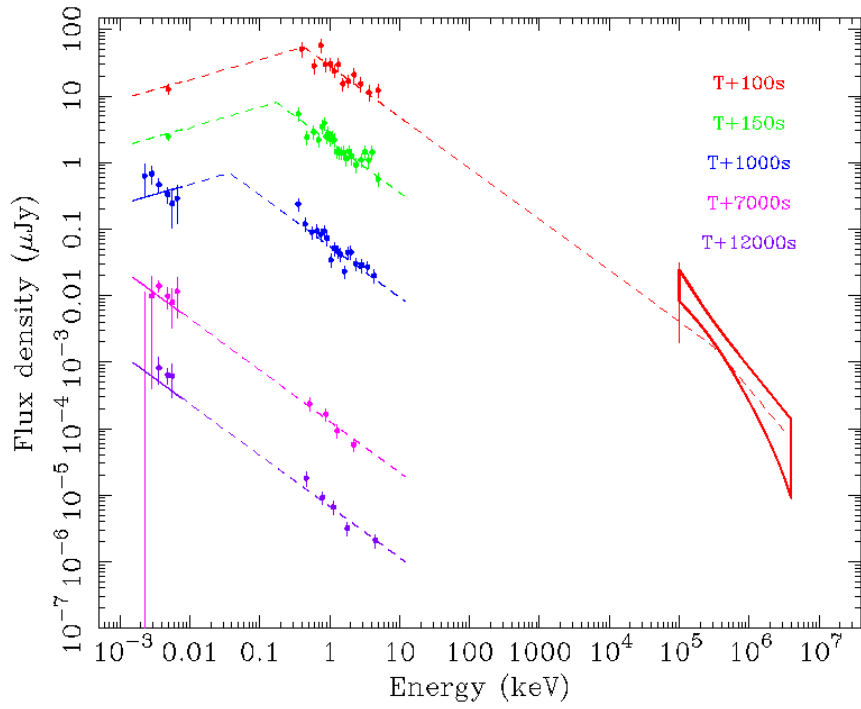


FIG. 3.— UVOT-XRT-LAT SEDs at different epochs, with the best fit shown (see text). The butterfly at 100s indicates the 68% confidence level region for the LAT flux, obtained from an unbinned likelihood analysis (95% error bar at 100 MeV is shown). Successive SEDs in time order are rescaled by 1:1, 1:10, 1:100, 1:1000, 1:10000.